J Membrane Biol (2007) 216:93–105
DOI 10.1007/s00232-007-9038-8

High-Level Expression, Refolding and Probing the Natural Fold of the Human Voltage-Dependent Anion Channel Isoforms I and II

Harald Engelhardt · Thomas Meins · Melissa Poynor · Volker Adams · Stephan Nussberger · Wolfram Welte · Kornelius Zeth

Received: 1 September 2006 / Accepted: 14 May 2007 / Published online: 9 September 2007

Abstract The voltage-dependent anion channel (VDAC) is the major protein found in the outer membrane of mitochondria. The channel is responsible for the exchange of ATP/ADP and the translocation of ions and other small metabolites over the membrane. In order to obtain large amounts of pure and suitably folded human VDAC for functional and structural studies, the genes of the human isoforms I and II (HVDAC1 and HVDAC2) were cloned in *Escherichia coli*. High-level expression led to inclusion body formation. Both proteins could be refolded *in vitro* by adding denatured protein to a solution of zwitterionic or nonionic detergents. A highly efficient and fast protocol for refolding was developed that yielded more than 50 mg of pure human VDACs per liter of cell culture. The native and functional state of the refolded porins was probed by Fourier transform infrared spectroscopy to determine the secondary structure composition and by electrophysiological measurements, demonstrating the pore-forming activity of HVDAC1. Furthermore, binding of HVDAC1 to immobilized ATP was demonstrated. Limited proteolysis of HVDAC1 protein embedded in detergent micelles in combination with matrix-assisted laser desorption ionization mass spectrometric analysis was applied to identify micelle-exposed regions of the protein and to develop an improved topology model. Our analysis strongly suggests a 16-stranded, antiparallel β-barrel with one large and seven short loops and turns. Initial crystallization trials of the protein yielded crystals diffracting to 8 Å resolution.

Keywords Mitochondrial porin · Membrane channel · Human voltage-dependent anion channel · Refolding

H. Engelhardt
Department of Molecular Structure Biology, Max Planck Institute of Biochemistry, Am Klopferspitz 18, D-82152 Martinsried, Germany

T. Meins · K. Zeth (✉)
Department of Membrane Biochemistry, Max Planck Institute of Biochemistry, Am Klopferspitz 18, D-82152 Martinsried, Germany
e-mail: zeth@biochem.mpg.de

M. Poynor · S. Nussberger
Biological Institute, Department of Biophysics, University of Stuttgart, Pfaffenwaldring 57, D-70550 Stuttgart, Germany

V. Adams
Clinics for Cardiology, Heart Center Leipzig, University Hospital, Russenstrasse 19, D-04289 Leipzig, Germany

W. Welte
Faculty of Biology, University of Konstanz, Universitätsstrasse 10, D-78457 Konstanz, Germany

Introduction

A pore-forming protein (porin) is involved in the exchange of adenosine triphosphate (ATP) and adenosine diphosphate (ADP) and the diffusion of small hydrophilic molecules across the outer mitochondrial membrane. Porins from mitochondria are known as voltage-dependent anion channels (VDACs) due to their anion-selective behavior in conductance measurements (Benz, 1994; Colombini, 1980). VDAC has binding sites for glycerol and hexokinase, provides these cytoplasmic enzymes with preferential access to ATP and couples oxidative phosphorylation with metabolic activation (Leterveer, Gellerich & Nicolay, 1995; Fiek et al., 1982). Moreover, VDAC forms complexes with mitochondrial creatine kinase, an enzyme localized in the intermembrane space (Brdiczka, Kaldis & Wallimann, 1994; Wallimann et al., 1992), and

with the adenine nucleotide translocator (ANT), which plays the key role in ATP/ADP exchange across the inner membrane (Beutner et al., 1998). VDAC was also detected in non-mitochondrial membranes of mammalian cells, i.e., in the plasma membrane of human B lymphocytes and in the membrane of the sarcoplasmic reticulum of human skeletal muscle. The protein therein may potentially carry out similar functions as regulated ion channels (Bathori et al., 2000).

Mitochondrial porin seems to play an essential role in early apoptosis events on the mitochondrial level (Green & Kroemer, 2004; Rostovtseva et al., 2005; Shoshan-Barmatz et al., 2006). There is evidence that mitochondrial porin and truncated Bid (tBid) upon complex formation can induce VDAC closure, leading to reduced metabolite exchange and mitochondrial dysfunction (Rostovtseva et al., 2004). Moreover, a complex of VDAC and ANT, also known as the permeability transition pore, may be controlled by the pro- and antiapoptotic molecules Bax and Bcl-2 and several proteinous factors from viruses. The formation of oligomeric Bax pores in the mitochondrial membrane also accounts for the efflux of cytochrome *c* or other proapoptotic factors from the intermembrane space and can provide an alternative way of outer membrane permeabilization (Kuwana et al., 2002).

Eukaryotic porins share only little, if any, detectable sequence similarity with their prokaryotic channel homologues, and they significantly differ in their oligomerization. However, both are of similar size and shape as revealed by cryoelectron microscopy and X-ray crystallography (Weiss et al., 1991; Guo & Manella, 1993; Hirsch et al., 1997). Another striking structural similarity between the two groups is the high content of β-sheets as revealed by Fourier transform infrared (FTIR) and circular dichroism (CD) spectroscopy (Abrecht et al., 2000; Shao, Kinnally & Manella, 1996). Secondary structure prediction algorithms (Vogel & Jähnig, 1986; Jeanteur, Lakey & Pattus, 1991; Haris & Chapman, 1992; Thinnes & Reymann, 1997) assign a high content of β-structure for both the mitochondrial and bacterial porins. Functional studies of VDAC and bacterial porins in black lipid membranes through conductivity measurements demonstrated similar single-channel conductance steps characteristic of black lipid membranes (Benz, 1985).

Despite the obvious functional importance of mitochondrial porins and the fact that bacterial porins have been studied much more intensively, structural determinations of VDACs at atomic resolution are not yet available. Corresponding investigations require suitable amounts of protein, which is often the limiting factor of human membrane proteins. To this end, we constructed expression systems for the human VDAC isoforms I (HVDAC1) and II (HVDAC2) and worked out the conditions for efficient refolding. We analyzed the secondary structure of renatured porin and probed the functional properties by conductance measurements and binding to immobilized ATP. We describe peptide mapping experiments for HVDAC1 used to evaluate the porin fold in detergent micelles, and we suggest an experimentally refined HVDAC1 topology model. Finally, initial crystallization conditions of HVDAC1 are presented.

Experimental Procedures

Chemicals and Media

Tryptone and yeast extract were purchased from Difco Laboratories (Augsburg, Germany). *N,N*-Dimethyldodecylamin-*N*-oxide (LDAO, 30% solution) was from Fluka (Deisenhofen, Germany); *n*-octyl-pentaoxyethylene (C8E5) and *n*-octyl-tetraoxyethylene (C8E4) were from Bachem (Heidelberg, Germany); and *n*-decyl-β-D-glucopyranoside (DEM), *n*-dodecyl-β-D-glucopyranoside (DDM) and *n*-octyl-β-D-glucopyranoside β-OG) were from Calbiochem (Bad Soden, Germany). ATP-agarose matrix 2767 and 6888 was purchased from Sigma-Aldrich (Munich, Germany), and isopropyl-β-D-thiogalactopyranoside (IPTG) was from BTS-BioTech Trade & Service (St. Leon-Roth, Germany). The endoproteinases trypsin, Lys-C, Glu-C and Asp-N were purchased from Sigma-Aldrich.

Cloning and Expression of HVDAC1 and HVDAC2

The DNA sequences of HVDAC1 and HVDAC2 were generated by polymerase chain reaction (PCR), using primers containing a *Bam*H1 and *Bgl*II restriction enzyme recognition site and a plasmid with the total coding sequence of both proteins (generous gift of Dr. M. Forte, Vollum Institute, Portland, OR). The PCR product was digested with *Bam*H1 and *Bgl*II and after gel purification cloned into the *Bam*H1, *Bgl*II restriction site of the PDS56/RBII-6xHis expression vector (Stuber et al., 1990). The correct orientation of the inserted DNA was confirmed by *Eco*RI digest of the isolated plasmid and direct sequence analysis.

High-Level Expression of Porin

For the large-scale production of HVDAC1 and HVDAC2, 20-ml overnight cultures of *Escherichia coli* M15(pREP4) containing the plasmids that encode the isoforms were used to inoculate 1 liter of LB medium, which consisted of 1%

bactotryptone, 0.5% yeast extract, 1% NaCl, 100 μg/ml ampicillin and 50 μg/ml kanamycin, adjusted to pH 7. Bacteria were grown at 37°C under aerobic conditions while shaking at 200 rpm to an optical density OD_{600} of 0.8–0.9 before IPTG was added to a final concentration of 1.0 mM. Incubation was continued for another 5–6 h to a final value of up to 2.5. Cells were harvested by centrifugation at 5,000 x *g* for 20 min at 4°C, resuspended in 60 ml of buffer A (150 mM NaCl, 30 mM Tris HCl, pH 8.0) and broken by two passages through a French press. Inclusion bodies were pelletised at 48,000 x *g* for 30 min and four times washed as follows. The viscous suspension was centrifuged at 48,000 x *g* for 30 min and the pellet resuspended and washed four times. The first two washing steps were carried out with 100 ml of buffer A using a Potter-Elvejhem homogenizer. The suspensions were centrifuged for 30 min at 48,000 x *g*. The third washing step was performed by resuspending the pellet in 50 ml of buffer A, containing 0.5 mg/ml of lysozyme and 1% of *n*-octylpolyoxyethylene, followed by incubation for 30 min at 30°C (homogenization and centrifugation as described above). A last washing step with 50 ml of buffer A removed lysozyme and *n*-octylpolyoxyethylene.

Refolding, Purification and Stability Determination

Inclusion bodies were solubilized in a 6 M guanidine HCl, 10 mM DTE, 0.1 mM ethylenediaminetetraacetic acid (EDTA) and 100 mM Tris HCl (pH 8) to a final protein concentration of 10–15 mg/ml. The latter was calculated by means of the absorption at 280 nm and the theoretical extinction coefficients of 36,960 $M^{-1}\,cm^{-1}$ and 65,890 $M^{-1}\,cm^{-1}$ for HVDAC1 and HVDAC2, respectively. Refolding was performed at 4°C by dropwise dilution of solubilized protein into refolding buffer containing 0.1 mM EDTA, 1 mM DTE, 100 mM Tris HCl (pH 8) and one of the following detergents: 2% LDAO, 1% DDM, 1% DEM, 2% ß-OG or 1.5% C8E5. The procedure was carried out at 4°C. Dilution was stopped when a final concentration of 0.4–0.5 M guanidine HCl was reached. Fractions of all solutions were kept at 4°C for up to 170 h, and small aliquots were taken to determine the A_{280} as an indicator of the protein amount that remained in solution after refolding. For further purification, the solution was centrifuged at 150,000 x *g* for 1 h, concentrated to approximately one-tenth of its original volume and dialyzed twice against buffer B (0.1% LDAO, 50 mM phosphate, pH 6) for 24 h. The solution was then diluted fivefold with dialysis buffer to reduce the LDAO concentration and to enhance protein binding to the nickel-nitrilotriacetic acid (Ni-NTA) matrix. The column with HVDAC1 bound was washed with five bed volumes of the same buffer and with five bed volumes of buffer B containing 50 mM imidazole. The protein was eluted with buffer B plus 300 mM imidazole. Fractions containing VDAC were finally pooled, concentrated and dialyzed against 20 mM Tris HCl (pH 8) plus the detergent used for further studies.

Binding Studies with ATP-Agarose

ATP-agarose was used to test the nucleotide-binding characteristics of the recombinant and refolded HVDAC1. Buffers and conditions were essentially those described in the literature (Florke et al., 1994; Hartman et al., 1992). A column containing 100 μl ATP-agarose was equilibrated with 1 ml of buffer E (0.5% C8E5, 50 mM acetic acid/sodium acetate, pH 5), loaded with approximately 100 μg of refolded HVDAC1 in buffer E and incubated at 4°C for 1 h. After washing with 1 ml buffer E, HVDAC1 was eluted with 50 mM ATP in buffer E.

Dynamic Light Scattering

Measurements of dynamic light scattering (DLS) were performed with a DynaPro-801 instrument (Protein Solutions, Charlottesville, VA). The protein solution with a concentration of 3–4 mg/ml was dialyzed against 0.35% C8E5 or 0.2% DDM in 20 mM Tris HCl buffer (pH 8). The solution (250 μl) was centrifuged at 180,000 x *g* and run through a filter of 20 nm exclusion limit prior to injection into the light-scattering cuvette. All measurements were performed at 18°C. The data returned from the instrument included scattering amplitude of the particle, a quantity proportional to the protein concentration and the translational diffusion coefficient. Intensity fluctuations of the 90° signal are indicative of particle motion (Schurtenberger & Newman, 1993). The particle radius and molecular mass were calculated assuming a spherical protein shape and using the Einstein-Stokes relation.

Attenuated Total Reflection FTIR

FTIR spectra were collected in a Nicolet FTIR 740 (Nicolet Analytical Instruments, Madison, WI) spectrometer applying the attenuated total reflection (ATR) technique. Aliquots (200 μl) of purified HVDAC1 and HVDAC2, each containing 0.35 mg protein, were dialyzed against 0.35% C8E4 and 10 mM phosphate buffer (pH 7) to remove buffer salts interfering with the amide I and II regions of the spectra. The samples were applied on a germanium crystal for ATR measurements and dried under

N_2 at room temperature. There were 512 scans accumulated at a resolution of 2 cm^{-1} before and after flushing the protein with N_2, saturated with D_2O for H-D exchange (60 min). The relative content of secondary structure elements was assessed using Fourier self-deconvolution for determination of the band positions (Kauppinen et al., 1981) and fitting for quantitative analyses (Byler & Susi, 1986; Arrondo et al., 1993).

Secondary Structure Prediction

The secondary structure prediction of the HVDAC1 sequence was performed using the Web-based server software TMBETA (http://www.psfs.cbrc.jp/tmbeta-net) and TMBB (http://www.bioinformatics.biol.uoa.gr/PRED-TMBB/). To compare the secondary structure content of HVDAC1 predicted with VDAC1 from *Saccharomyces cerevisiae*, the two sequences were aligned to each other by homology and the secondary structure content was thereby assigned.

Proteolytic Digestion of HVDAC1

Digest of HVDAC1 embedded in detergent micelles was performed with the proteases trypsin, Lys-C, Glu-C and Asp-N. Approximately 100 μg of the protein in 0.5% C8E4, 1 mM mercaptoethanol and 50 mM 4-(2-hydroxyethyl)-1-piperazineethanesulfonic acid (HEPES)/NaOH (pH 7) were treated with 1–5 μg of the proteases in 25 mM HEPES/NaOH (pH 7) and incubated at 30°C. Samples of approximately 20 μg were taken after 1, 4 and 24 h; frozen in liquid N_2; and stored at –20°C for subsequent matrix-assisted laser desorption ionization mass spectrometric (MALDI-MS) determination.

MALDI-MS Analysis of Proteolytic Peptides

MALDI-MS experiments were carried out with a Bruker Biflex (Bruker Daltonics, Bellerica, MA) TOF mass spectrometer. The samples were prepared according to the dried-droplet method: 1-μl samples were mixed with 9 μl of solution containing HCCA matrix (23 mg/ml) in acetonitrile plus 0.1% trifluoroacetic acid at a ratio of 2:1. Pure matrix (2 μl) was spotted on a 3-mm^2 stainless steel target and dried. A 1-μl aliquot of the sample matrix solution was spread on the crystalline matrix and desiccated as above. The target was then inserted into the ion source, and spectra of all peptides were collected. Approximately 100 single laser shots per sample were accumulated and averaged.

Reconstitution of HVDAC1 in Planar Bilayer Membranes

The experiments were performed as described in Benz (1994) and Ahting et al. (2001). Planar lipid membranes were formed from a 1% (w/v) solution of diphytanoyl-phosphatidylcholine (Avanti Polar Lipids, Alabaster, AL) dissolved in *n*-decane/butanol (9:1 v/v), spread across a circular hole (area about 1 mm^2) in the thin wall of a Teflon cell that separates two aqueous compartments filled with 1 M KCl solution. HVDAC1 (1–10 μg) solubilized in 0.5% *n*-octylpolyoxyethylene and 20 mM phosphate buffer (pH 7) was added, and voltages of ±10 m*V* to ±100 m*V* were applied. Membrane currents were measured with a pair of Ag/AgCl electrodes (World Precision, Berlin, Germany or Metrohm, Herisau, Germany) using a HEKA EPC8 amplifier (HEKA, Lambrecht, Germany) or a Keithley 428 current amplifier (Keithley Instruments, Cleveland, OH). Amplified signals were filtered at 3 kHz, monitored with an analog/digital storage oscilloscope and recorded with a strip chart recorder or alternatively digitized with a CED 1401 analog/digital converter (Cambridge Electronic Design, Cambridge, UK) and recorded and stored on a personal computer using the WinEDR version 2.4.8 software package (J. Dempster, University of Strathclyde, Glasgow, UK). Single-channel analysis was carried out using the Origin 7.5 (OriginLab Corporation, Nothhampton, MA) software package.

Three-Dimensional Crystallization of HVDAC1

Samples of HVDAC were concentrated to approximately 20 mg/ml in different detergents (1% β-OG, 0.8% *n*-octylpolyoxyethylene, 0.3% DEM), and crystallization trials were performed against crystal screens I and II and the Index Screen (Hampton Research), using 2 μl protein plus 0.75 μl precipitant hanging drops. Native crystals were directly frozen from the screening drops and tested at beamline ID14-EH4 of the synchrotron radiation source (European Synchrotron Radiation Facility, Grenoble, France). Data were collected at 100 K and diffraction patterns recorded on an ADSC Q4R mosaic charge-coupled device detector system (European Synchrotron Radiation Facility, Grenoble, France).

Results

Expression, Purification and Refolding of HVDAC1 and HVDAC2

C-terminally histidine-tagged isoforms I and II of human VDAC were overproduced in *E. coli* at high levels, yielding

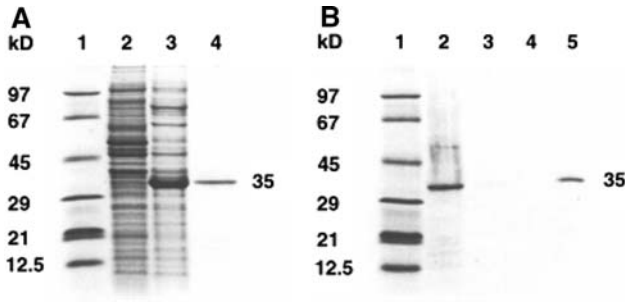

Fig. 1 SDS-PAGE analysis of HVDAC1 purification and binding to ATP-agarose. **a** *Lane 1*, Molecular mass markers; *lane 2*, whole-cell fraction of *E. coli* cells before induction with IPTG; *lane 3*, whole-cell fraction after induction with 1 mM IPTG; *lane 4*, protein sample after refolding of the protein and Ni-NTA affinity chromatography. VDAC runs at an apparent molecular weight of 35 kDa. All samples were heated at 95°C for 10 min before application. The gel was stained with Coomassie brilliant blue. **b** *Lane 1*, Molecular mass markers; *lane 2*, HVDAC1 sample before application of ATP-agarose; *lane 3*, elution of unbound protein confirming that HVDAC1 was completely bound to the column; *lane 4*, sample of the washing step, which was applied to remove unspecifically bound protein; *lane 5*, protein eluted with 50 mM ATP in a sodium acetate/acetic acid buffer system. Samples were heated at 95°C in sample buffer for 10 min after precipitation with cold acetone

up to 100 mg of unfolded protein per liter of cell culture. Figure 1a shows sodium dodecyl sulfate-polyacrylamide gel electrophoresis (SDS-PAGE) analysis of the whole-cell extract before (lane 2) and after (lane 3) induction with 1.5 mM IPTG for 5–6 h. HVDAC1 runs at 35 kDa. Inclusion bodies were purified and quantitatively solubilized in 6 M guanidine HCl. Refolding was achieved by continuously dropping porin sample into solutions of nonionic or zwitterionic detergents. All five detergents chosen apparently induced folding and insertion of the protein into protein-detergent micelles. Nevertheless, the amount of soluble protein and its stability in solution were dependent on the detergent used (*see* Table 1). The overall concentration of soluble protein in the supernatant was determined after 1 h, 24 h and 1 week, as shown in Table 1. The highest amount of soluble HVDAC1 was obtained with 2% LDAO in our Tris HCl buffer system with a yield of up to 90%. The success of apparent folding was 70% recovery using the nonionic detergent DDM or DEM and negligible with ß-OG and C8E5. The long-term stability of both isoforms was therefore sufficient in the presence of LDAO, DDM and DEM. The refolded protein was finally purified via Ni-NTA agarose chromatography in a one-step procedure, which also was applied for the exchange of LDAO against detergents of higher critical micellar concentration. The amount of purified protein was approximately 50 mg per liter of culture medium after the single chromatographic step. Lane 4 in Figure 1a shows the isolated and purified protein which was used for all biochemical and biophysical experiments described afterward.

Table 1 Yield of soluble HVDAC1 after refolding

Detergent for refolding					
	2% LDAO	1% DDM	1% DEM	1% C8E4	2% β-OG
1 h	90%	75%	70%	30%	15%
24 h	80%	70%	70%	30%	15%
170 h	80%	60%	55%	30%	10%

HVDAC1 was refolded in the presence of the zwitterionic detergent LDAO and the nonionic detergents DDM, DEM, C8E4 and β-OG. The detergent concentrations are given in percent (v/v). The amount of soluble and folded protein was determined by the protein absorption at 280 nm

Identification of Physiological Function: The ATP Binding Site

In order to verify that the soluble form of HVDAC1 represented the protein in its functional conformation, we applied specific binding tests. The SDS-PAGE analysis in Figure 1b illustrates that refolded HVDAC1, containing an ATP-binding site, reversibly bound to two types of ATP-agarose. In the case shown, ATP was covalently coupled to agarose via the C9 position of the nucleotide. In another experiment, ATP was linked via the ribose hydroxyl group with an 11-atom spacer in between. After loading the affinity matrix with HVDAC1, the column was extensively washed to remove unbound protein. HVDAC1 remained completely immobilized to the column and could be eluted in both cases only with ATP (Fig. 1b, lane 5), illustrating the specific binding. In contrast to these studies, NADH-linked agarose did not bind HVDAC1 under corresponding conditions.

Reconstitution into Artificial Planar Bilayer Membranes

To prove the functional state of refolded HVDAC1, we added highly purified porin to the *cis* side of a bilayer membrane and recorded the conductance at voltages in the range –100 to 100 m*V*. Figure 2a shows conductance steps upon insertion of the porin into the membrane at 10 m*V* with a characteristic size of approximately 5 nS. Current measurements of single porin channels demonstrated the ability of refolded HVDACI to switch between an open and closed state (Fig. 2b). The membrane conductance between these two states differed by approximately 2.0 nS. Insertion of multiple porins in a membrane allowed determination of the voltage dependence of refolded HVDACI. At membrane potentials of ±10 m*V*, the closing events in the channel recordings represented only a minor fraction of the current fluctuations. At larger voltages, the number of

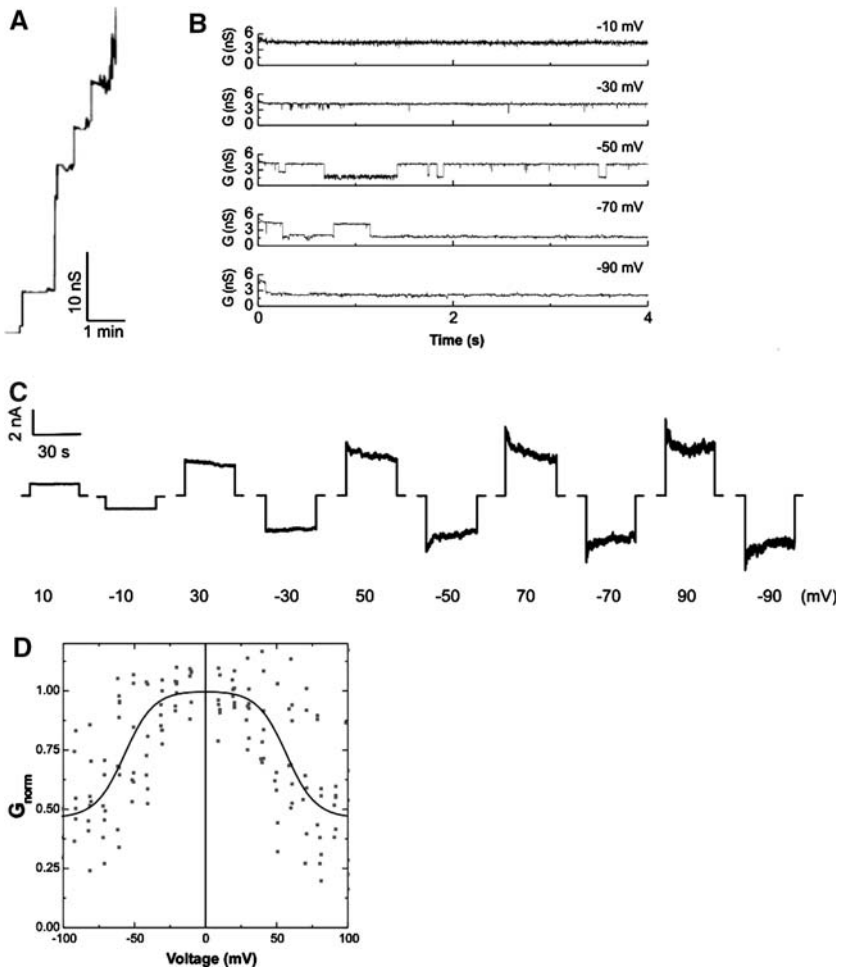

Fig. 2 Recordings of channel conductance after addition of HVDAC1 to a lipid bilayer membrane. The lipid bilayer experiments were performed by adding the sample to one side (*cis* side) of the membrane formed by diphytanoyl-phosphatidylcholine/*n*-decane in 1 M KCl, 10 mM HEPES (pH 7.2) solution. Different voltages were applied, and the current across the membrane was recorded. **a** The conductance increased in discrete steps, indicating incorporation of a single porin. Applied voltage: 10 m*V*. **b** Sample current traces of single-channel recordings after voltage jumps from 0 m*V* to the voltages indicated. **c** Samples of current traces of multiple channels incorporated into a membrane recorded after voltage jumps from 0 m*V* to the voltages indicated below the traces. **d** Channel conductance, *G*, as a function of transmembrane potential. The conductance at a given voltage was divided by the mean conductance determined at 10 and –10 m*V*. A Boltzmann distribution (*solid curve*) was fitted to the data. The midpoint potential of the distribution was at roughly ±57 m*V*

closing events increased and the steady-state membrane currents decreased (Fig. 2c). The steady-state conductance of HVDAC1, obtained from experiments in which a few channels were reconstituted into the membrane, showed a bell-shaped curve as a function of the applied voltage (Fig. 2d). It followed the Boltzmann distribution and indicated that 50% of HVDAC1 switched to a closed substate at about 57 ± 8 m*V*.

Secondary Structure Analysis, DLS and Crystallization Attempts

In order to determine the secondary structure of the HVDAC isoforms and the oligomeric state, ATR-FTIR spectroscopy and DLS were applied. Figure 3 displays the spectra recorded for HVDAC1 and HVDAC2 before and after H-D exchange. The amide I band maxima close to 1,630 cm^{-1} are typical for a high content of β-sheet structure (Arrondo et al., 1993). Apart from this dominant band, a further characteristic but weaker band appeared around 1,656 cm^{-1} (Fig. 3d) indicating α-helical content. The shoulder at 1,695 cm^{-1} is strongly indicative of an antiparallel β-sheet and, thus, provides clues to the arrangement of β-strands. Secondary structure prediction was performed using recently developed Web servers. The predicted amounts are very close to the experimental values of 47.9% and 41.3%, respectively, although they deviate depending on the approach chosen. The predicted α-helical content is in reasonable agreement with the values of about 7% for isoform I and 10% for isoform II as assessed by FTIR.

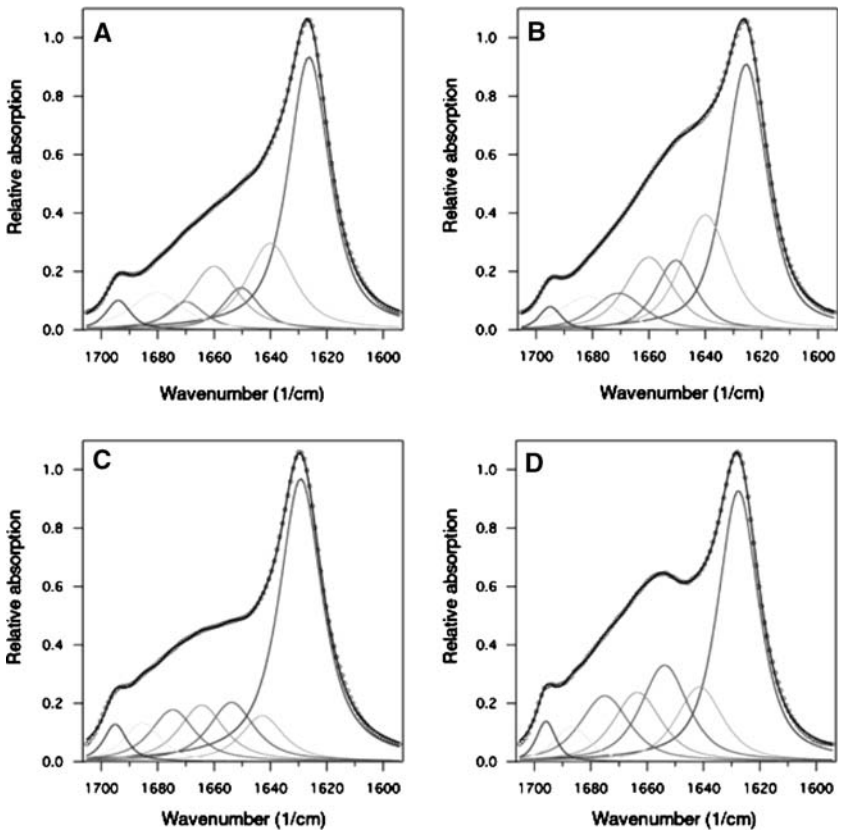

Fig. 3 ATR-FTIR absorbance spectra (amide I band) of HVDAC1 and -2. **a,b** Spectra of HVDAC1. **c,d** Spectra of HVDAC2. **a,c** Samples from H_2O solutions, **b,d** samples after 60-min hydrogen-deuterium exchange. The dominant band at 1,630 cm^{-1} identifies β-sheet structure. The shoulder at 1,695 cm^{-1} is indicative of antiparallel β-sheets and the band centered around 1,652 cm^{-1} after H-D exchange for α-helix. The sum of all absorption bands (*line*) fits to the spectrum of the porin (*open circles*)

We also performed DLS measurements to evaluate the size of particles in solution. The signal revealed a homogeneous distribution of molecules in both samples tested and returned an estimated molecular mass of porin-detergent micelles of about 68 kDa. The baseline values (*data not shown*) are compatible with the actual size to be monodispersed by the size distribution fit. To further prove the homogeneity of the refolded HVDAC1 samples, we attempted three-dimensional crystallization of the protein. Protein crystals under a variety of conditions appeared and were tested using the synchrotron. Crystals obtained under the condition 30% polyethylene glycol 4000, 0.1 M Na-acetate (pH 4.6), 0.2 M ammonium acetate and 0.8% n-octylpolyoxyethylene (OPOE) 50 x 20 x 50 µm in size showed a rectangular shape and diffracted weakly to 8 Å resolution (*data not shown*).

Peptide Mapping Analysis and Topology Modeling

Characterization of the HVDAC1 topology was performed by partial proteolysis of the solubilized porin and subsequent mass spectrometric mapping of the peptides generated. Proteolytic degradation was performed with the endoproteinases trypsin, Lys-C, Asp-N and Glu-C. Samples were taken after 1, 4 and 24 h and analyzed by MALDI-MS. Trypsin degradation yielded nine, Lys-C ten, Asp-N six and Glu-C protease seven peptides, with masses close or identical to those calculated from the protein sequence. The results are summarized in Table 2. The proteolytic peptides partially coincide well with predicted positions of β-strands and exhibit an amphipathic character typical for the membrane-spanning region of β-sheets (see Fig. 4). We identified 17 single cleavage sites or regions with more than one site, including the N and C termini which were accessible to the proteases. Two regions assigned as turns/loops by secondary structure predictions contained a single Glu-C site but were not attained by the protease, and one turn, consisting of the amino acids A, G and P, provided no cleavage site at all. Most of the 26 remaining cleavage sites fell into predicted β-strands with an amphipathic pattern and were, thus, assumed to be hidden by detergents or inaccessible inside the channel. This view of a stably formed β-barrel is in accordance with FTIR spectra of the digested porin that still shows a dominant, although slightly reduced, band at 1,630 cm^{-1}, indicative of an intact β-sheet structure (*spectrum not shown*). Neighboring loops were usually separated by two amphipathic β-strands of 8–11 residues, enclosing a turn or loop located at the opposite surface of the porin. The relative amount of β structure in our model is 47.5% for HVDAC1, which reflects the results of FTIR analysis and secondary structure predictions (Table 3).

Table 2 Identification of proteolytic fragments from HVDAC

Trypsin			Lys-C		
Exp. determined mass $(M+H)^+$	Calculated mass $(M+H)^+$	Peptide fragment	Exp. determined mass $(M+H)^+$	Calculated mass $(M+H)^+$	Peptide fragment
854.9	854.5	24–31	1,324.7	1,323.7	24–35
1,374.5	1,375.5	67–77	1,695.2	1,683.8	65–77
2,177.5	2,176.0	78–96	1,457.9	1,456.7	165–177
1,214.5	1,213.6	167–177	4,040.4	4,037.9	165–200
2,601.7	2,600.2	178–200	4,381.0	4,379.1	165–203
359.4	359.2	201–203	2,601.9	2,600.2	178–200
1,947.4	1,946.0	204–221	2,945.2	2,941.4	178–203
1,819.1	1,817.9	205–221	2,536.1	2,533.3	204–227
2,104.6	2,103.2	240–259	2,104.9	2,103.2	240–259
1,104.2	1,103.6	278–287	3,116.9	3,114.8	240–269
			2,014.7	2,013.6	278–294
			2,792.8	2,790.4	270–294
Asp-N			Glu-C		
Exp. determined mass $(M+H)^+$	Calculated mass $(M+H)^+$	Peptide fragment	Exp. determined mass $(M+H)^+$	Calculated mass $(M+H)^+$	Peptide fragment
1,557.9	1,557.9	19–32	2,285.2	2,285.2	13–33
2,434.3	2,434.2	81–102	983.5	983.4	63–69
3,570.0	3,570.0	92–123	1,794.8	1,793.8	63–76
2,103.2	2,102.1	161–179	3,699.8	3,698.9	92–124
3,186.7	3,184.6	161–188	1,261.7	1,261.7	93–103
1,881.1	1,883.9	189–205	2,102.0	2,102.0	162–180
3,090.6	3,090.5	267–294	2,966.5	2,966.5	181–206
			1,430.7	1,430.7	284–294

HVDAC1 was proteolytically degraded by the four proteases trypsin, Lys-C, Asp-N and Glu-C. The peptide mass of the fragments was analyzed by MALDI-MS. The experimentally determined masses are compared with the theoretically potential masses under the assumption of specific protease cleavage. The experimentally derived masses were assigned to the corresponding peptide fragments

Interestingly, two consecutive cleavage sites including a proline (DPDA sequence), which appears to be situated in one larger loop (sequence position 231–234), were not attacked by Asp-N and Glu-C. We must assume that this loop is folded such that it is at least partly inaccessible to proteases. The longest loop of the protein was assigned to amino acids 91–125. Our topology model revealed some properties of the distribution of certain amino acids that appear to be quite reasonable. Many of the aromatic residues (e.g., Tyr25, Tyr70, Phe74, Phe134, Tyr149, Trp152, Phe160, Tyr176 and others) are found close to the ends of β-strands (Fig. 5) and may be arranged to form aromatic girdles as in bacterial outer membrane proteins. Furthermore, all of the proline residues (Pro139, Pro232, Pro256) appear around or within turn regions and at the beginning of the N-terminal helix (Pro7, Pro8). The resulting topology diagram of HVDAC1 with 16 β-strands as displayed in Figure 5 is based mainly on the results of peptide mapping analysis but also on secondary structure analysis and the concept of amphipathicity for membrane-embedded β-strands.

Discussion

Successful approaches have already been described but were mainly restricted to bacterial outer membrane proteins (Buchanan, 1999). The two human membrane proteins HVDAC1 and HVDAC2 investigated here were overproduced in *E. coli* and could be refolded with high efficiency and yield. Our protocol for renaturation of these mitochondrial porins varies from procedures described for bacterial porins (Eisele & Rosenbusch, 1990; Pullen et al., 1995; Schmid, Kromer & Schulz, 1996) and the VDAC homologue from *Neurospora crassa* (Koppel et al., 1998; Shi et al., 2003) and from other procedures described for the renaturation of HVDAC1 and the *Drosophila melanogaster* porin DmPorin2 (Aiello et al., 2004). In our study, HVDAC1 and HVDAC2 were solubilized in guanidine HCl and refolded through rapid dilution in the presence of mild zwitterionic or nonionic detergents, which increased the yield by a factor of approximately 5 compared to other approaches (Shi et al., 2003; Koppel et al., 1998). The

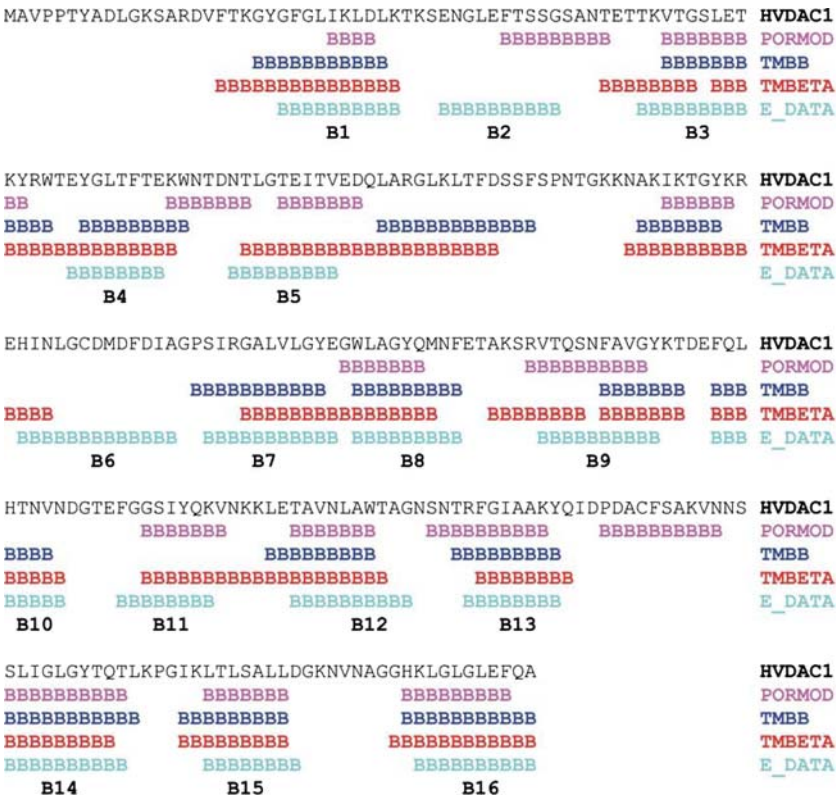

Fig. 4 Sequence alignment of the mitochondrial porins HVDAC1. *Underlined regions* (...BB…) of HVDAC1 indicate β-strands (B1-B16) based on different tools used to address β-strands to the primary structure. PORMOD indicates β-strands predicted for the HVDAC1 homologue VDAC1 from *S. cerevisiae* according to Casadio et al. (2002). TMBETA and TMBB servers were used to compare experimental data (E_DATA) with data of two established protein prediction servers

Table 3 Secondary structure composition of HVDAC1 and HVDAC2

	α-Helix content (%)		β-Strand content (%)	
	Determined FTIR	Predicted	Determined FTIR	Predicted TMBETA/TMBB
HVDAC1	6.6	–	47.9	61/46
HVDAC2	10.4	–	41.3	61/46

The α-helix and β-sheet contents according to ATR-FTIR measurements are compared with values assessed through secondary structure prediction programs TMBETA and TMBB

success of refolding appears to be correlated with the hydrophobic length of the detergent. DDM or LDAO with C_{12} chains yielded higher amounts than C8E5 or β-OG, which possess C_8 chains only. The propitious influence of long-chain detergents on the yield of refolded OmpF from *E. coli* was already observed (Eisele & Rosenbusch, 1990). We speculate that longer alkyl chains may match the hydrophobic portion of the natural membrane of 3–4 nm thickness better than C_8 compounds do.

The native structure of refolded HVDAC1 was probed by several methods. All our investigations provided evidence that the porin adopted a fully functional conformation. The refolded porin showed a uniform size distribution and diffusion behavior in DLS experiments and crystallized in two dimensions with a good lateral regularity as shown previously (Dolder et al., 1999), indicating homogeneity and an intact conformational state. Moreover, our initial three-dimensional crystallization attempts prove that the recombinant protein is able to pack into a three-dimensional lattice and is accessible for X-ray crystallography, even though at medium resolution of 8 Å. HVDAC1 specifically bound to ATP-agarose, indicating that the ATP-binding site existed in a functional form and was accessible. The single-channel conductance of refolded HVDAC1 compares well with that obtained for recombinant HVDAC1 purified from yeast mitochondria (4.1 nS; Blachly-Dyson et al., 1993) or porin 31HL isolated from human B-lymphocyte membranes (4.3 nS; Benz & Brdiczka, 1992; Benz, 1994). At a voltage above ±50 m*V*, the channels revealed an additional subconductance state of roughly 2.3 nS (Fig. 2b), which indicated the existence of at least two states (Benz, 1994; Colombini, 1980; Leterveer et al., 1995; Benz et al., 1992). The voltage dependence of refolded HVDAC1 thus conformed with that of

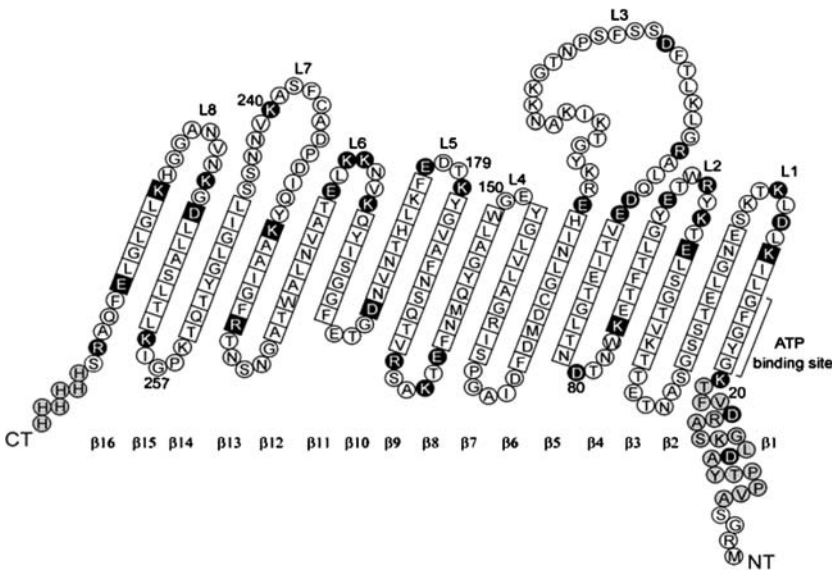

Fig. 5 Proposed folding model for the β-barrel structure of HVDAC1. View from the membrane-exposed side of the 16-stranded (β1-β16) β-barrel and the eight loops (L1-L8). The N-terminal α-helix and the C-terminal His-tag are marked in *gray*. Residues supposed to lie in the integral membran domain are *boxed*. The cleavage sites of the four proteases identified by peptide mapping and MALDI-MS are marked in *black*

mitochondrial porins from other sources, which switch to 50% of their initial conductance between 35 and 90 m*V* (Benz, 1994). The properties of refolded HVDAC1 channels were thus consistent with the voltage dependence of most mitochondrial porins studied so far.

Contrary to experiments with many bacterial porins, which usually run as trimers in SDS-PAGE if treated at room temperature (Engelhardt et al., 1990), oligomers of purified HVDAC1 have never been detected under these conditions. On the other hand, the molecular mass calculated for HVDAC1 (solubilized in 0.35% C_8E_4) from DLS measurements was $\sim$68 kDa and is obviously not in good agreement with the sequence-derived mass of 32 kDa for the monomer. The higher molecular mass as determined by DLS can be explained by the fact that a significant number of detergent molecules are firmly attached to the protein, thereby mimicking an increased overall molecular mass.

A number of structural models for VDAC have been proposed based on a pore organization similar to that of bacterial porins, with a distinct number of β-strands and one α-helix together with various biochemical and analytical data (Blachly-Dyson et al., 1990; De Pinto et al., 1991; Rauch & Moran, 1994; Shao et al., 1996; Song et al., 1998; Casadio et al., 2002; Aiello et al., 2004; Colombini, 2004; Yehezkel et al., 2006). Independent FTIR measurements revealed the expected high content of antiparallel β-sheet and appropriate amounts of α-helix for both isoforms. The values of $\sim$48% (41%) β structure and 7% (10%) α-helix for HVDAC1 (HVDAC2) are in good agreement with the secondary structure composition of the related porins (Koppel et al., 1998; Abrecht et al., 2000; Ahting et al., 2001) and are similar to values of 45% β-sheet and 12% α-helix obtained for refolded ncVDAC by CD spectroscopy (Koppel et al., 1998). However, they differ significantly from the 60.8% β-sheet and 17.9% α-helix determined for HVDAC1 using CD spectroscopy by Shi et al. (2003). Because of the high similarity/identity (71/30%) between HVDAC1 and ncVDAC, a similar secondary structure composition was expected and confirmed for the human channel. Moreover, a recently published study using FTIR-ATR measurements on two isolated and purified plant isoforms of VDAC determined 50–53% β-sheet further verifies our results (Abrecht et al., 2000). More interesting in structural terms is the absolute content of β structure in porins because it provides clues as to the number and length of β-strands. In HVDAC1, 135 amino acids are expected to form β-sheets, yielding an average β-strand length of about nine residues, assuming a 16-stranded β-barrel. In the *Paracoccus denitrificans* porin, about 154 amino acids are involved in β-barrel formation, indicating that the 16 β-strands have an average length of 9.6 ± 2.5 amino acids (5 and 15 being the extremes), while the corresponding values for Omp32 are higher (average length 12.8 ± 3.0; Zeth et al., 2000) and illustrate a certain variability in porin β-barrel architecture (204 amino acids in 16 β-strands of 7–18 amino acids in length, with an average of 12.8 ± 3.0), probably due to the differing membrane environment.

The lengths and positions of β-strands of HVDAC1 were determined by a combination of structure prediction and limited proteolysis of solubilized HVDAC1. The crucial assumption was that only regions of the membrane protein that are not covered by detergents are accessible to proteolytic attack and can also be taken as being exposed in the natural membrane. These regions should include loops, turns and the N-terminal α-helix, which is not membrane-embedded according to antibody studies (De Pinto et al., 1991; De Pinto & Palmieri, 1992). Our assumption is

corroborated by Bühler et al. (1998), who analyzed the protease accessibility of the porin from *Rhodobacter capsulatus* and ScrY from *Salmonella typhimurium* and found that all proteolytic sites of these proteins were localized in loop regions only. This applies for Omp32 that was digested while inserted in the outer membrane (Gerbl-Rieger et al., 1992; Zeth et al., 2000). Proteolytic attack occurred inside loops or close to both ends of β-strands, which in is agreement with our alignment. The number of β-strands derived and proposed here is 16, which agrees with other models (De Pinto & Palmieri, 1992; Rauch & Moran, 1994; Abrecht et al., 2000; Casadio et al., 2002; Aiello et al., 2004), with an average length of 8.6 amino acids per β-strand. This is in the lower range of bacterial porins but reflects the average value of nine suggested for two plant VDAC isoforms (Abrecht et al., 2000). Out of 15 loops or turns plus the two termini that should be accessible to proteolytic attack in a 16-stranded ß-barrel, we could identify 12 plus the terminal regions by the location of one or multiple protease cleavage sites. Interestingly, one of the putative but uncleaved loops, possessing a Glu-C cleavage site (Glu53), was cut by protease V8 and identified by N-terminal sequencing in a similar approach of De Pinto et al. (1991), so 15 regions of exposed sites can be regarded as experimentally established. Only the two putative loops/turns AGP (positions 137–139) and EG (150–151) were not detected in proteolysis experiments. The sequence AGP does not contain a cleavage site but is predicted to be a loop, while the turn EG is probably too short to allow proteases to bind; actually, it is the smallest turn found in our model. In Figure 4, our model, based mainly on experimental evidence, is compared with secondary structure algorithms and a three-dimensional model of VDAC from *S. cerevisiae*. These results differ in terms of β-strand number and sequence obtained by the various methods applied. The N-termial region (residues 1–80) in particular is difficult to characterize as it shows an increased internal disorder (*data not shown*), and a definite proof of secondary structure using common bioinformatic tools is therefore more complex. Our model hence overlaps significantly better in the C-terminal part of models developed based on the programs TMBETA and TMBB. Both programs predict 14 β-strands with slightly differing location. Other models in the literature proposed for VDAC proteins range from 12- to 19-stranded structures. The 12-stranded model from the *S. cerevisiae* porin (Blachly-Dyson et al., 1990) predicts the α-helical domain at the N terminus (residues 1 - 23) to be fully embedded in the lipid or detergent environment. We find three cleavage sites (Asp8, Asp15, Lys19) in this region and agree with the conclusion that the helix is exposed to the plasma or buffer solution (De Pinto et al., 1991; Rauch & Moran, 1994; Casadio et al., 2002). Furthermore, some of the proteolytic sites found in HVDAC1 (e.g., Lys28, Lys30, Lys32, Glu59, Lys61) that correspond to residues of the yeast homologue were thought to be buried in the membrane (Blachly-Dyson et al., 1990). We therefore suppose that the 12-stranded model contains a number of uncertainties and does not represent the natural fold. The model of Song et al. (1998), as suggested for VDAC from *N. crassa* and used as a reference for the porin from rat liver mitochondria (Yehezkal et al., 2006) and human VDAC1 (Colombini, 2004), assumes the existence of 13 β-strands together with a membrane-inserted N-terminal α-helix. Again, this model is in critical conflict to our protease studies since nine cleavage sites are clearly located inside expected membrane domains and most of the protected cleavage sites are found in loop regions. The 19-stranded model (Forte, Guy & Mannella, 1987), which was based on computer algorithms, has the general drawback of β-barrels with an odd number of β-strands. In such barrels, at least two β-strands are parallel and cannot build a smooth barrel wall, which would create a discontinuity of less stability. This is probably why all known β-barrels of membrane proteins possess even numbers of β-strands. Our data rather support other models (De Pinto et al., 1991; Rauch & Moran, 1994; Thinnes & Reymann, 1997; Abrecht et al., 2000; Casadio et al., 2002; Aiello et al., 2004) as to the number of β-strands, the accessibility of the termini and some of the suggested loop regions. But there are also significant differences. Firstly, about six cleaving sites identified by our experiments are located in the center of membrane-spanning β-strands in the model of De Pinto et al. (1991). Secondly, the first large loop thought to be accessible to proteases in the latter model possesses four cleavage sites for trypsin that were assumed to be attacked. But they were not cleaved in our experiments. The discrepancy may derive from the difference in accuracy of mass determinations of peptides, i.e., gel electrophoresis and MALDI-MS as used here. This finding may also have consequences for the assignment of antibody binding sites in HVDAC (Thinnes & Reymann, 1997). Rauch & Moran (1994) used a particularly designed algorithm to identify β-strands in porins that was apparently successful for the *R. capsulatus* porin. However, the prediction suggested that amino acids 98–107 (numbering with respect to Fig. 5) represented a membrane β-strand in HVDAC1, a region that was cleaved by two proteases in our experiments. The results of combined secondary predictions, peptide mapping and mass spectroscopic identification of peptides enabled us to establish a folding model of HVDAC1 (Fig. 5) that suggests the existence of one large loop (91–125), which could be equivalent to loop L3 from bacterial porins and may add to the channel characteristics of mitochondrial porins.

Structure predictions together with chemical modifications or proteolytic analyses offer clues for structure

modeling but cannot replace structure determination. With the large-scale purification and refolding approach at hand, we see a chance to solve the structure of the human porins by X-ray crystallography or nuclear magnetic resonance spectroscopy.

Acknowledgment We very much thank Dr. Jason Breed for critical reading of the manuscript. The help of Joachim Diez at the beginning of the project is gratefully acknowledged. Dr. Michael Forte enabled us to start the porin project by providing us with the cDNA. The help of the beamline staff at the Joint ESRF and EMBL Structural Biology Group (JSBG) beamlines of the European Synchrotron Radiation Facility (Grenoble, France) is greatly appreciated.

References

Abrecht H, Goormaghtigh E, Ruysschaert JM, et al. (2000) Structure and orientation of two voltage-dependent anion-selective channel isoforms – an attenuated total reflection Fourier-transform infrared spectroscopy study. J Biol Chem 275:40992–40999

Aiello R, Messina A, Schiffler B, et al. (2004) Functional characterization of a second porin isoform in *Drosophila melanogaster*. J Biol Chem 279:25364–25373

Arrondo JLR, Muga A, Castresana J, et al. (1993) Quantitative studies of the structure of proteins in solution by Fourier-transform infrared spectroscopy. Prog Biophys Mol Biol 59:23–56

Ahting U, Thieffry M, Engelhardt H, et al. (2001) Tom40, the pore-forming component of the protein-conducting TOM channel in the outer membrane of mitochondria. J Cell Biol 153:1151–1160

Bathori G, Parolini I, Szabo I, et al. (2000) Extramitochondrial porin: facts and hypotheses. J Bioenerg Biomembr 32:79–89

Benz R (1985) Porin from bacterial and mitochondrial outer membranes. CRC Crit Rev Biochem 19:145–190

Benz R (1994) Permeation of hydrophilic solutes through mitochondrial outer membranes –review on mitochondrial porins. Biochim Biophys Acta 1197:167–196

Benz R, Brdiczka D (1992) The cation-selective substrate of the mitochondrial outer membrane pore. Single-channel conductance and influence on intermembrane and peripheral kinases. J Bioenerg Biomembr 24:33–39

Benz R, Maier E, Thinnes FP, Götz H, Hilschmann N (1992) Studies on human porin VII. The channel properties of the numan B-lympcyte membrane-derived 'Porin 31HL' are similar to those of mitochondrial porins. Biol Chem Hoppe-Seyler 373:295–303

Beutner G, Ruck A, Riede B, et al. (1998) Complexes between porin, hexokinase, mitochondrial creatine kinase and adenylate translocator display properties of the permeability transition pore. Implication for regulation of permeability transition by the kinases. Biochim Biophys Acta 1368:7–18

Blachly-Dyson E, Peng SZ, Colombini M, et al. (1990) Selectivity changes in site-directed mutants of the VDAC ion channel – structural implications. Science 247:1233–1236

Blachly-Dyson E, Zambronicz EB, Yu WH, et al. (1993) Cloning and functional expression in yeast of two human isoforms of the outermitochondrial membrane channel, the voltage-dependent anion channel. J Biol Chem 268:1835–1841

Brdiczka D, Kaldis P, Wallimann T (1994) In vitro complex formation between the octamer of mitochondrial creatine kinase and porin. J Biol Chem 269:27640–27644

Buchanan SK (1999) Beta-barrel proteins form bacterial outer membranes: structure, function and refolding. Curr Opin Struct Biol 9:455–461

Bühler S, Michels J, Wendt S, et al. (1998) Mass spectrometric mapping of ion channel proteins (porins) and identification of their supramolecular membrane assembly. Proteins 2:63–73

Byler DM, Susi H (1986) Examination of the secondary structure of proteins by deconvoluted FTIR spectra. Biopolymers 25:469–487

Casadio R, Jacoboni I, Messina A, et al. (2002) A 3D model of the voltage-dependent anion channel (VDAC). FEBS Lett 520:1–7

Colombini M (1980) Structure and mode of action of a voltage-dependent anion-selective channel (VDAC) located in the outer mitochondrial membrane. Ann N Y Acad Sci 341:552–563

Colombini M (2004) VDAC: the channel at the interface between mitochondria and the cytosol. Mol Cell Biochem 256/257:107–115

De Pinto V, Prezioso G, Thinnes F, et al. (1991) Peptide-specific antibodies and proteases as probes of the transmembrane topology of the bovine heart mitochondrial porin. Biochemistry 30:10191–10200

De Pinto V, Palmieri F (1992) Transmembrane arrangement of mitochondrial porin or voltage-dependent anion channel (VDAC). J Bioenerg Biomembr 24:21–26

Dolder M, Zeth K, Tittmann P, et al. (1999) Crystallization of the human, mitochondrial voltage-dependent anion-selective channel in the presence of phospholipids. J Struct Biol 127:64–71

Engelhardt H, Gerbl-Rieger S, Krezmar D, et al. (1990) Structural properties of the outer membrane and the regular surface protein of *Comamonas acidovorans*. J Struct Biol 105:92–105

Eisele JL, Rosenbusch JP (1990) In vitro folding and oligomerization of a membrane protein. Transition of bacterial porin from random coil to native conformation. J Biol Chem 265:10217–10220

Fiek C, Benz R, Foos N, et al. (1982) Evidence for identity between the hexokinase-binding protein and the mitochondrial porin in the outer membrane of rat liver mitochondria. Biochim Biophys Acta 688:429–440

Florke H, Thinnes FP, Winkelbach H, et al. (1994) Channel-active mammalian porin, purified from crude membrane fractions of human B-lymphocytes and bovine skeletal muscle, reversibly binds adenosine-triphosphate (ATP). Biol Chem Hoppe-Seyler 375:513–520

Forte M, Guy HR, Mannella CA (1987) Molecular genetics of the VDAC ion channel. Structural model and sequence analysis. J Bioenerg Biomembr 19:341–350

Gerbl-Rieger S, Engelhardt H, Peters J, et al. (1992) Topology of the anion-selective porin Omp32 from *Comamonas acidovorans*. J Struct Biol 108:14–24

Guo XW, Manella CA (1993) Conformational change in the mitochondrial channel, VDAC, detected by electron cryomicroscopy. Biophys J 64:545–549

Green DR, Kroemer G (2004) The pathophysiology of mitochondrial cell death. Science 305:626–629

Hartman J, Huang Z, Rado TA, et al. (1992) Recombinant synthesis, purification, and nucleotide-binding characteristics of the 1st nucleotide-binding domain of the cystic-fibrosis gene product. J Biol Chem 267:6455–6458

Hirsch A, Breed J, Saxena K, et al. (1997) The structure of porin from *Paracoccus denitrificans* at 3.1 Angstroem resolution. FEBS Lett 404:208–210

Haris PI, Chapman D (1992) Does Fourier-transform infrared spectroscopy provide useful information on protein structures? Trends Biochem Sci 17:328–333

Jeanteur D, Lakey JH, Pattus F (1991) The bacterial porin superfamily: sequence alignment and structure prediction. Mol Microbiol 5:2153–2164

Kauppinen JK, Moffatt DJ, Mantsch HH, et al. (1981) Fourier self-deconvolution – a method for resolving intrinsically overlapped bands. Appl Spectrosc 35:271–276

Koppel DA, Kinnally KW, Masters P, et al. (1998) Bacterial expression and characterization of the mitochondrial outer membrane channel. Effects of N-terminal modifications. J Biol Chem 273:13794–13800

Kuwana T, Mackey MR, Perkins G, et al. (2002) Bid, Bax, and lipids cooperate to form supramolecular openings in the outer mitochondrial membrane. Cell 111:331–342

Leterveer FD, Gellerich FN, Nicolay K (1995) Macromolecules increase the channeling of ADP from externally associated hexokinase to the matrix of mitochondria. Eur J Biochem 232:569–577

Pullen JK, Liang SM, Blake MS, et al. (1995) Production of *Haemophilus influenzae* type-B porin in *Escherichia coli* and its folding into the trimeric form. Gene 152:85–88

Rauch G, Moran O (1994) On the structure of mitochondrial porins and its homologies with bacterial porins. Biochem Biophys Res Commun 200:908–915

Rostovtseva TK, Anonsson B, Suzuki M, et al. (2004) Bid, but not Bax, regulates VDAC channels. J Biol Chem 279:13575–13583

Rostovtseva TK, Tan W, Colombini M (2005) On the role of VDAC in apoptosis: fact and fiction. J Bioenerg Biomembr 37:129–142

Schmid B, Kromer M, Schulz GE (1996) Expression of porin from *Rhodopseudomonas blastica* in *Escherichia coli* inclusion bodies and folding into exact native structure. FEBS Lett 381:111–114

Schurtenberger P, Newman M (1993) Characterization of Biological and Environmental Particles Using Static and Dynamic Light Scattering, vol. 2. Boca Raton, FL: Lewis

Shao L, Kinnally KW, Manella CA (1996) Circular dichroism studies of the mitochondrial channel, VDAC, from *Neurospora crassa*. Biophys J 71:778–786

Shi S, Jiang C, Chen Q, et al. (2003) One-step on-column affinity refolding purification and functional analysis of recombinant human VDAC1. Biochem Biophys Res Commun 303:475–482

Shoshan-Barmatz V, Israelson A, Brdiczka D, Sheu SS (2006) The voltage-dependent anion channel (VDAC): function in intracellular signalling, cell life and cell death. Curr Pharamceut Design 12:2249–2270

Song J, Midson C, Blachly-Dyson E, et al. (1998) The topology of VDAC as probed by biotin modification. J Biol Chem 273:24406–24413

Stuber D, Bannwarth W, Pink JRL, et al. (1990) New B-cell epitopes in the *Plasmodium falciparum* malaria circumsporozoite protein. Eur J Immunol 20:819–824

Thinnes FP, Reymann S (1997) New findings concerning vertebrate porin. Naturwissenschaften 84:480–498

Vogel H, Jähnig F (1986) Models for the structure of outer membrane proteins of *Escherichia coli* derived from Raman spectroscopy and prediction methods. J Mol Biol 190:191–199

Wallimann T, Wyss M, Brdiczka D, et al. (1992) Intracellular compartmentation, structure and function of creatine kinase isoenzymes in tissues with high and fluctuating energy demands – the phosphocreatine circuit for cellular energy homeostasis. Biochem J 281:21–40

Weiss MS, Kreusch A, Schiltz E, et al. (1991) The structure of porin from *Rhodobacter capsulatus* at 1.8 Å resolution. FEBS Lett 280:379–382

Yehezkel G, Hadad N, Zaid H, et al. (2006) Nucleotide-binding sites in the voltage-dependent anion channel. J Biol Chem 281:5938–5946

Zeth K, Diederichs K, Welte W, et al. (2000) Crystal structure of Omp32, the anion-selective porin from *Comamonas acidovorans*, in complex with a periplasmic peptide at 2.1 Angstroem resolution. Structure 8:981–992